# Fractal boundaries in open hydrodynamical flows: Signatures of chaotic saddles

Áron Péntek,[1,*] Zoltán Toroczkai,[1,†] Tamás Tél,[1] Celso Grebogi,[2,3,4] and James A. Yorke[2,4]
[1]*Institute for Theoretical Physics, Eötvös University, Puskin utca 5-7, H-1088 Budapest, Hungary*
[2]*Department of Mathematics, University of Maryland, College Park, Maryland 20742*
[3]*Institute for Plasma Research, University of Maryland, College Park, Maryland 20742*
[4]*Institute for Physical Science and Technology, University of Maryland, College Park, Maryland 20742*
(Received 12 December 1994)

We introduce the concept of fractal boundaries in open hydrodynamical flows based on two gedanken experiments carried out with passive tracer particles colored differently. It is shown that the signature for the presence of a chaotic saddle in the advection dynamics is a fractal boundary between regions of different colors. The fractal parts of the boundaries found in the two experiments contain either the stable or the unstable manifold of this chaotic set. We point out that these boundaries coincide with streak lines passing through appropriately chosen points. As an illustrative numerical experiment, we consider a model of the von Kármán vortex street, a time periodic two-dimensional flow of a viscous fluid around a cylinder.

PACS number(s): 05.45.+b, 47.10.+g, 47.15.Ki, 47.27.Cn

## I. INTRODUCTION

Advection of passive tracer particles in open nonstationary flows has attracted recent interest [1–11] because even in simple time periodic cases the tracer particles can exhibit chaotic motion. Here we shall consider two-dimensional viscous flows around obstacles with the property that the flow is *time periodic* close to the obstacle and uniform far away from it (both before and behind the obstacle). We address questions, like how the boundary between regions colored differently changes when going downstream along the flow, that can lead to a better understanding of transport and mixing in open flows. We claim that the fractal structure of the boundary is a signature for the presence of *nonattracting chaotic sets* [14], *chaotic saddles* for short, in the tracer dynamics along the flow.

Assuming incompressibility, the equations of motion for a passively advected dye particle in the $(x, y)$ plane have the form (the so-called Lagrangian dynamics)

$$\dot{x} = v_x \equiv \frac{\partial \psi(x,y,t)}{\partial y}, \qquad \dot{y} = v_y \equiv -\frac{\partial \psi(x,y,t)}{\partial x}, \quad (1)$$

where $v_x$, $v_y$ are the two components of the velocity field, and $\psi$ is the time-dependent stream function that plays in this problem the role of a Hamiltonian. This form allows us to characterize passive transport in Navier-Stokes flows with a system of two ordinary differential equations that are far easier to solve than the Navier-Stokes equations, provided an exact or approximate form of the velocity field or $\psi$ is available. More generally speaking, the solution of the Navier-Stokes flow is an input, e.g., in the form of the stream function, to Eq. (1) that itself represents a dynamical system describing particle advection. We shall use an approximate function $\psi$ whose form is chosen to fit certain aspects of what is observed in numerical simulations of the Navier-Stokes equation. The chaotic motion we investigate is generally *robust*, and we believe that most of its features should be present in the original Navier-Stokes flow. The system (1) can be solved far more quickly with an approximate but analytically given $\psi$ than with the Navier-Stokes velocity field determined numerically, and still requires extensive computation.

If the flow were stationary, Eq. (1) would correspond to a one-degree-of-freedom autonomous Hamiltonian problem that is always integrable. With a time-dependent velocity field, however, Eq. (1) has the same structure as that of a driven one-degree-of-freedom Hamiltonian system that is known to be nonintegrable. In the language of hydrodynamics, stream lines and particle trajectories coincide in stationary flows only, and in nonstationary cases the latter can be complicated even if the instantaneous stream lines are smooth curves [1]. We shall restrict our attention to the simplest nonstationary case, to time periodic flows, that makes a convenient description of the dynamics possible in the form of taking snapshots at integer multiples of the period, a *stroboscopic map*.

By choosing the reference frame in such a way that the obstacle, whose linear size is of order unity, is situated around the origin, the velocity field becomes both space and time independent for $|x|, |y| \gg 1$. The particle motion in the flow is in such cases very much like a scattering process [12,13] with the trajectories being scattered by the vortices and the obstacle. Incoming tracer particles may exhibit complicated motion in the wake and exit after a finite amount of time. Since the flow far away

*Present address: Institute for Pure and Applied Physical Sciences, University of California at San Diego, La Jolla, CA 92093-0075.
†Present address: Department of Physics, Virginia Polytechnic Institute and State University, Blacksburg, VA 24061.

 

from the obstacle is uniform, the asymptotic motion of the particles is well defined.

To visualize the dynamics of the passive tracer particles colored differently and help to understand the dynamics, let us imagine two experiments with such flows (see Fig. 1). In each experiment we present a version (i) that can be carried out also in a laboratory and another one (ii) that is devoted solely to numerical investigations.

*Experiment A: the "inflow" (two-fluid) experiment.* (i) Inject dye particles continuously into the flow far in front of the obstacle along the line $x \equiv x_{in} < 0$, $\mid x_{in} \mid \gg 1$, so that the colors above and below a critical $y_c$ are different (say, black and white), as illustrated in Fig. 1(a). Investigate how the boundary between the two colors evolves in time. Since the pattern will stabilize to a periodically oscillating structure, it is convenient to take snapshots at multiple integers of the period of the flow. Depending on the choice of the initial coordinate $x_{in}$ we shall call such stationary boundaries (at fixed $y_c$) $x_{in}$ boundaries. We emphasize that these boundaries are *physical observables.* (ii) In an alternative way that can only be realized numerically, the boundaries can also be obtained by following the *time reversed* Lagrangian dynamics of particles sprinkled in a domain around the obstacle and coloring the initial points of trajectories in the backward dynamics, depending on whether after crossing the $x = x_{in}$ line they lie above or below $y_c$.

*Experiment B: the "outflow" (two-exit) experiment.* (i) Sprinkle dye particles in a domain around the obstacle. Save their initial coordinates in a computer and take a video record of their trajectories until they cross a line $x \equiv x_{out} \gg 1$ far away downstream. Color the initial points (observed on a stroboscopic map) depending on whether after crossing the $x = x_{out}$ line they lie above or below a preselected value $y_c$ [cf. Fig. 1(b)]. The boundary between particles colored differently will be called (at fixed $y_c$) the $x_{out}$ boundaries. These boundaries are thus also *physical observables.* (ii) In an alternative way that can only be realized numerically, they can also be obtained as the boundaries in the *time reversed* Lagrangian dynamics of particles continuously injected into the flow at the final coordinate $x_{out}$ so that the colors for $y > y_c$ and $y < y_c$ are different.

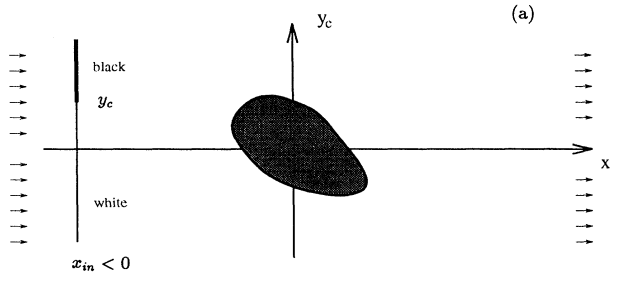


Experiment A

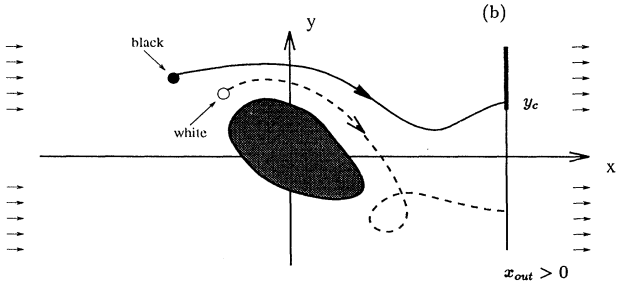


Experiment B

FIG. 1. Schematic diagram illustrating experiments A (a) and B (b).

The full equivalence of methods (i) and (ii) for generating a given type of boundary would require the return to the initial point when applying methods (i) and (ii) to the same trajectory subsequently. This exact return is never the case, however, the initial point and the end point of the combined trajectory of (i) and (ii) can have identical $y$ coordinates (and slightly different $x$ coordinates), provided the line of inflow or outflow is in the asymptotic region: $\mid x_{in} \mid, \mid x_{out} \mid \gg 1$. This is due to the asymptotic homogeneity of the flow, i.e., to the fact that stream lines and particle trajectories are straight lines in the region $x \leq x_{in}$ or $x \geq x_{out}$. In such cases the boundaries obtained by methods (i) and (ii) coincide. Later in the paper we consider boundaries where the line of inflow or outflow conditions is close to the obstacle so that $\mid x_{in} \mid$ or $x_{out}$ are of order unity. For example, one can take $x_{in} = 0$, $y_c = 1$ which corresponds to injecting tracer particles on top of the obstacle. In such cases the methods (i) and (ii) are still well defined but need not lead to exactly the same result: only the fractal parts of the boundaries will be identical.

The aim of this paper is to show that one can obtain in both experiments complicated *fractal boundaries* as a consequence of the *chaoticity* of the tracer dynamics. Because of the Hamiltonian character of Eq. (1) no chaotic attractor can be present, but in such cases there often exists at least one *chaotic saddle* in a bounded region of the flow [7–11] generating transient chaos [14]. For simplicity, we talk below about the stroboscopic map rather than the periodic flow. The chaotic saddle is then the set of points near which tracer particles can stay for an arbitrarily long time. Such a set has a stable and an unstable *manifold* ("manifold" in this case is a "curve"). The *stable* manifold is an invariant curve along which the saddle can be reached after an infinitely long time. Under a stroboscopic map it appears as a curve winding in a complicated manner. The *unstable* manifold is the stable manifold of the time reversed Lagrangian dynamics. Both of these manifolds are *fractal* curves. We shall see that the fractal parts of the $x_{in}$ and $x_{out}$ boundaries in experiments A and B coincide with parts of or the full unstable and stable manifold of the same chaotic set, respectively.

The paper is organized as follows. In the next section we extend the concept of fractal boundaries to any open Hamiltonian system and give the connection between this

notion and the $x_{in}$ and $x_{out}$ boundaries of experiments A and B. It is shown that the fractal properties should be independent of the choice of $x_{in}$ or $x_{out}$ in a broad range of inflow or outflow conditions, respectively. Sec. III is devoted to the description of the particular analytical model we use. The numerical results obtained for the $x_{in}$ and $x_{out}$ boundaries, the chaotic saddle, and their fractal dimensions are presented in Sec. IV. Section V contains our concluding remarks.

## II. FRACTAL BOUNDARIES IN OPEN HAMILTONIAN SYSTEMS

Fractal boundaries [15,16] were originally defined in dissipative systems possessing attractors. If two or more attractors coexist, their basins of attraction might be separated by boundaries that are fractals. We say that (for two-dimensional maps) a boundary is "fractal" at a point if arbitrary near that point contains infinitely many curves. The consequence is that trajectories starting in the vicinity of a fractal boundary exhibit very complicated and unpredictable motion before settling down into one of the possible quite simple attractors. Fractal basin boundaries are typically parts of *stable manifolds* of one or more *chaotic saddles*, situated between the attractors. It is worth noting that fractal basin boundaries have also been found in the advection problem of flows with sinks and sources [17] whose Lagrangian dynamics is thus non-Hamiltonian.

The presence of basin boundaries is not necessarily restricted to the existence of attractors in some bounded region of the phase space. One step to extend the concept of fractal boundaries to Hamiltonian systems has been made by Bleher, Grebogi, Ott, and Brown [18], who investigated the escape from a billiard and a potential well by distinguishing trajectories exiting via two different holes and different directions, respectively. The role of the attractors in dissipative cases is played in these systems by the two different long time asymptotics (exits through two different holes) available for trajectories.

We claim that a basin boundary can be defined in any open scattering system where the asymptotic part of the phase space can be divided in an appropriate way into two or more disjoint subsets. These subsets will be called the *exit regions* [18] and the boundary between them the *partitioning surface* (or line). Because of the uniqueness of the dynamics also the nonasymptotic part of the phase space can be divided in different regions, according to the different modes of exit at infinity. The boundary between them can be smooth or fractal. Of course, it is not hard to realize that the boundary in the nonasymptotic region is exactly the preimage of the partitioning surface taken in the $t = -\infty$ limit.

Due to the time reversal invariance of Hamiltonian systems, we can also define boundaries in the backward dynamics. One then takes a partitioning surface in the incoming asymptotic region whose image for $t = \infty$ will be the boundary. Both types of boundaries can be treated on equal footing.

The key observation of our paper is that the partitioning can be chosen arbitrarily from a continuum of possibilities provided the dynamics has a chaotic saddle and the partitioning surface crosses the stable or unstable manifold of this set. Figure 2(a) shows schematically the double foliation of the phase space provided by the manifolds of the chaotic saddle. Let us consider a stroboscopic map and follow the forward (backward) dynamics of the partitioning surface. The stable (unstable) manifold is the set of points that converge to the chaotic saddle as time goes forward (backward). Segments of the partitioning surface lying between the filaments of the stable (unstable) manifold will be transported in the forward (backward) dynamics to the outgoing (incoming) region so that asymptotically they *accumulate on the filaments of the unstable (stable) manifold.*

The way in which the local convergence to these manifolds takes place is illustrated in Fig. 2(b). For the sake of simplicity we consider one element of the chaotic saddle, a hyperbolic fixed point only, and investigate the forward dynamics. The partitioning surface is the boundary between two incoming regions colored black and white, respectively, and it is assumed to cross the stable manifold of the fixed point. The union of all images of the partitioning line forms a curve wildly oscillating when approaching the unstable manifold of the fixed point. The intersection points between the stable manifold and the boundary converge exponentially fast towards the fixed point with a convergence rate equal to the eigenvalue of the linearized dynamics. Consequently, the length of the lobes that are formed also increases exponentially in order to preserve volume. Therefore an infinite number of *differently colored layers* accumulate on the stable manifold that is itself part of the boundary. The extension of the layers is narrower the more unstable the periodic orbit is.

In general we can say that the boundary contains the full unstable (stable) manifold or parts of it. If the partitioning line taken in the incoming (outgoing) asymptotics crosses all the branches of the stable (unstable) manifold extending to infinity, the full unstable (stable) manifold of the chaotic set will lie on the boundary. The shape of this fractal part of the boundary is then *independent* of the partitioning line's position. If the partitioning line crosses only partially the stable (unstable) manifold, the boundary contains certain branches of the other manifold only. The fractal dimension of the boundary is, however, the same as in the previous case and thus independent of the choice of the partitioning line.

It can happen that there are two or more chaotic saddles present in the system. The fractal part of the basin boundary then can contain parts of any of the sets' unstable (stable) manifolds. The fractal dimension of the boundary will then coincide with the dimension of one of the sets' manifolds.

The boundary contains in any case a nonfractal part too: filaments accumulating on the fractal component and also some others extending smoothly to infinity. A boundary is fractal if it contains a fractal component. If the partitioning line does not intersect the stable (unstable) manifold at all, it is *not fractal* and does not appear as the invariant manifolds of the chaotic set.

In our hydrodynamical problem, experiment A (B) directly corresponds to the Hamiltonian situation described above. Because of the asymptotic homogeneity of the flow, the use of a line of inflow (outflow) conditions with $|x_{in}|, x_{out} \gg 1$ is the same as taking a partitioning line $\{x \leq x_{in}, y = y_c\}$ ($\{x \geq x_{out}, y = y_c\}$) in the asymptotic incoming (outgoing) region.

As a consequence of these general arguments we conclude that both the $x_{in}$ and $x_{out}$ boundaries in the hydrodynamical experiments A and B can contain a nonfractal and a fractal part. The latter only exists if the advection problem is chaotic and there is a chaotic saddle near the obstacle. The fractal part of the boundary in Experiment A (B) coincides with parts of the unstable (stable) invariant manifold of the chaotic set. The nonfractal part of the boundaries describes the convergence toward the chaotic set and can strongly depend on the choice of $x_{in}$, $x_{out}$, or $y_c$, i.e., on the type of inflow or outflow conditions, respectively.

At this stage it is worth comparing our results with another concept, *streak lines* that are common means for visualization of flows. They are defined as [19] the set of points reached, at a given instant of time, by an ensemble of particles previously injected at a given point into the

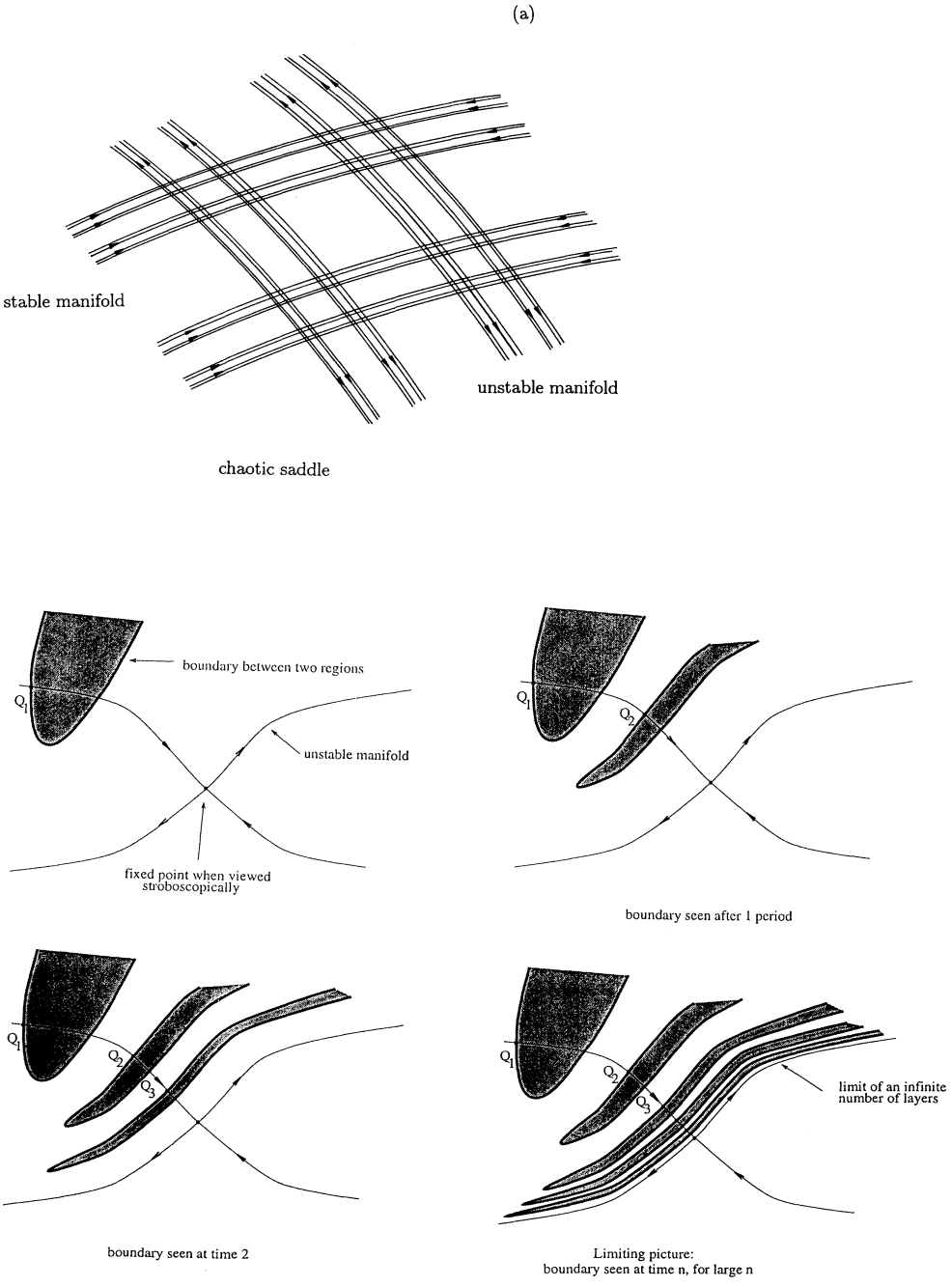


FIG. 2. Schematic diagram illustrating the convergence to the chaotic saddle of a general Hamiltonian system. (a) The chaotic saddle and its stable and unstable manifolds. A finite segment of the partitioning line (not shown) would be smoothly deformed before reaching the chaotic set. Points lying on the stable (unstable) manifold remain, however, glued to the set forever. Segments in between become more and more elongated, transported out to infinity so that they converge to the unstable (stable) manifold. (b) The evolution of the local structure of the boundary between two incoming regions black (B) and white (W) on a stroboscopic map when the partitioning line crosses the stable manifold of a fixed point. Once $Q_1$ is on the boundary, so must $Q_2, Q_3, \ldots$ be also on the boundary; thus the fixed point's unstable manifold is the limit of an infinite number of layers of the boundary. An analogous structure is built up in the $x_{in}$ boundary of the hydrodynamical experiment A around the chaotic saddle's unstable manifold.

flow. Thus, a streak line passing through a point $(x, y)$ is the curve traced out by nondiffusive tracer particles injected into the flow at $(x, y)$ continuously. While in steady flows, streak lines, streamlines, and particle trajectories coincide, they are different in time-dependent velocity fields and provide different ways of flow visualization. In such cases streak lines are also time dependent. They often appear as complicatedly winding fractallike curves on photographs taken at a given any instant of time [19] and have recently been analyzed also in the context of chaotic advection [3,9,10]. We note that the particle line emanated from $(x_{in}, y_c)$ form a streak line. Thus we conclude that the boundary (*both* the smooth and the fractal components) in experiment A is the streak line passing through $(x_{in}, y_c)$. By introducing the concept of time reversed streak lines as the streak lines of the backward Lagrangian dynamics, we can analogously say that the boundary in experiment B is the time reversed streak line passing through $(x_{out}, y_c)$.

The chaotic saddle, present in the dynamics, is solely responsible for the mixing property and chaotic behavior observed in the particle advection problem. Thus it is important to investigate not only its manifolds but also the set itself, as will be done in the case of the model flow presented below. In a laboratory experiment, the chaotic saddle can also be visualized by plotting the common part of the stable and unstable manifolds. An alternative way is provided by recording trajectories with a long lived chaotic behavior and performing a time series analysis to reconstruct the chaotic set [20].

## III. MODEL

As an example we consider the case of a circular obstacle, and study the particle motion around a cylinder. We shall work in a range of parameters where a von Kármán vortex street exists, where several streak line visualization experiments are available [19]. This problem has also been investigated numerically in detail from the point of view of chaotic dynamics [6–10]. For simplicity we shall take an analytical model system for the stream function introduced in Ref. [8]. It describes a situation when two vortices are present in the wake of the cylinder at any instant of time, and these vortices alternate when separating from the cylinder. The velocity field is then strictly time periodic with period $T$. The form of the analytical model is motivated by the results of a direct numerical simulation of the Navier-Stokes flow at Reynolds number 250 in a channel containing a cylinder in the middle, reported in Ref. [7]. The model describes certain quantitative features of the flow, like, e.g., the nearly marginally stable particle dynamics in the vicinity of the surface. Some other features, like, e.g., the width of the boundary layer, are chosen so that they deviate from that characterizing the Navier-Stokes flow. The reason for these differences lies in numerical convenience. A broader boundary layer makes the hyperbolic periodic orbits coming into this layer less unstable.

One of our aims is to illustrate with this model system that streak lines can be easily obtained by considering them as boundaries of the direct or time reversed Lagrangian particle dynamics. The numerical efforts needed to construct them in this way is much less than that needed by other methods applied to the same model. Therefore, this method might provide a useful tool also for determining streak lines in velocity fields obtained by direct numerical simulations.

In fulfilling the other objective, i.e., visualizing the chaotic saddle, other numerical tools are needed. It turns out that the *proper interior maximum* (PIM) triple method [21] successfully meets this need, and gives a much better resolution than by naively taking the common part of the stable and unstable manifolds. Unfortunately, the PIM triple method cannot be directly applied to experiments. However, the fractal boundaries are a diagnostics for the existence of the chaotic saddle.

The analytic model is defined by a stream function

$$\psi(x, y, t) = f(x, y)\, g(x, y, t), \tag{2}$$

where the first factor

$$f(x, y) = 1 - \exp\left\{-a[(x^2 + y^2)^{1/2} - 1]^2\right\} \tag{3}$$

yields the correct no slip boundary condition at the cylinder's surface whose center is chosen to lie at the origin. The cylinder radius has been taken to be unity, which can always be done by a suitable rescaling of the lengths introduced in the problem. The coefficient $a^{-1/2}$ plays the role of the width of the boundary layer.

The factor $g$ contains the contributions of the vortices and of the background flow with velocity $u_0$. It reads

$$g(x, y, t) = -wh_1(t)g_1(x, y, t) + wh_2(t)g_2(x, y, t) + u_0 y s(x, y). \tag{4}$$

The first two terms describe the alternating birth, evolution, and damping of vortices 1 and 2 of equal strength but opposite sign. The quantities $w$ and $h_i(t)$ stand for the overall vortex strength and amplitudes, respectively. Because of the alternating character, one has $h_2(t) = h_1(t - T/2)$, where $T$ denotes the time period of the flow. By choosing the time unit to be $T$, the amplitude function $h$ of the model takes the form

$$h_1(t) = |\sin(\pi t)|\,. \tag{5}$$

The vortex centers are assumed to move parallel to the $x$ axis and with a constant velocity. Their $x$ coordinates are expected to change with time as

$$x_1(t) = 1 + L[t \mod 1], \tag{6}$$

$$x_2(t) = x_1(t - 1/2), \tag{7}$$

while the $y$ coordinates are constants,

$$y_1(t) = -y_2(t) \equiv y_0. \tag{8}$$

Both vortices travel a distance $L$ during a period and then die out. Thus when vortex 1 is created at $(x = 1, y = y_0)$ at time zero, vortex 2 is just in its most developed state at $(x = 1 + L/2, y = y_0)$. The contribution of

the vortices to the stream function is represented by the form

$$g_i(x,y,t) = \exp\left(-R_0\{[x - x_{in}(t)]^2 + \alpha^2[y - y_c(t)]^2\}\right), \tag{9}$$

where $R_0^{-1/2}$ is the characteristic linear size of the vortices and $\alpha$ denotes the ratio, telling us how much longer is the linear size of the vortices along the $x$ axis as compared with the linear size along the $y$ axis.

The last term in Eq. (4) gives the contribution to the stream function by the background flow with uniform velocity $u_0$. The factor

$$s(x,y) = 1 - \exp\left[-(x-1)^2/\alpha^2 - y^2\right] \tag{10}$$

is introduced in order to simulate the shielding of the background flow just behind the cylinder. This is taken into account by using the same elongation factor $\alpha$ as in the case of the vortices.

The numerical values for the parameters are chosen in such a way that one obtains behind the cylinder a qualitative agreement with the known solution [7] of the Navier-Stokes problem. For Re = 250 this is fulfilled with $\alpha = 2, R_0 = 0.35, L = 2$, $y_0 = 0.3$, $u_0 = 14$, and $w = 24$. The width of the boundary layer is taken to be $a = 1$. At this point the model definitely deviates from parameters of the Navier-Stokes flow, but the qualitative results do not depend essentially on the particular value of $a$, and the choice is motivated just by numerical convenience. The model is tailored for simulating the flow in the wake behind the cylinder; nevertheless, here we use it in a broader sense both upstream and downstream. Our aim is not so much the study of the relevance of the particular model in this extended region, but rather to investigate the invariant chaotic saddles and the different types of boundaries that they generate.

## IV. NUMERICAL RESULTS

We carry out experiments A and B with the model system numerically, and determine the invariant sets.

### A. Experiment A

We start particles on a grid of 800 × 666 points in the rectangle shown in Fig. 3(a) and mark the initial

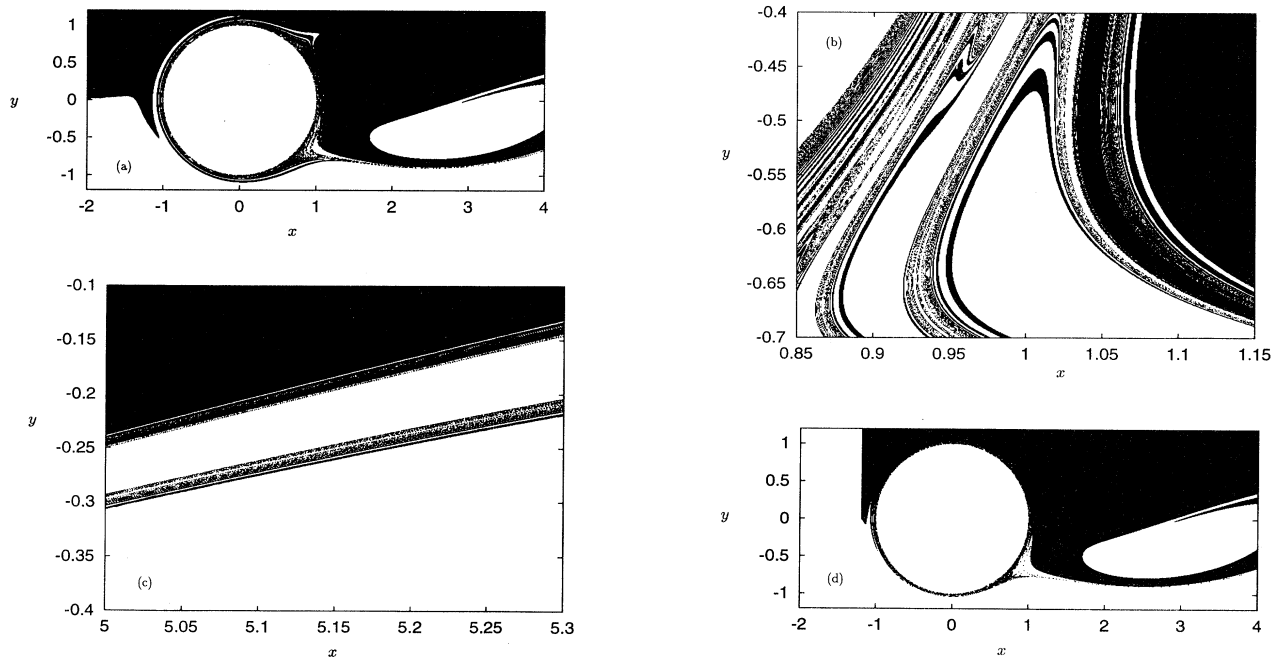


FIG. 3. The $x_{in} = -6$ boundary in experiment A with $y_c = 0$. (a) Particles were started on an $800 \times 666$ grid in the rectangle shown and iterated backward. They are marked "black" or "white" depending on whether, after crossing the $x = -6$ line on the stroboscopic map, they lie in the upper or lower half-plane, respectively. The snapshot is taken at time $t = 0.3$, relative to the stream function defined in the text. This particular instant of time was chosen because the vortices are then of approximately equal size. (b),(c) Enlargements of the two regions of (a) showing the fractal structure of the boundary. Parts of the boundary, where solid "white" regions meet solid "black" regions, belong to the nonfractal part, i.e., the boundary is a simple curve there. Such a structure can be observed in (a) below and above the cylinder. Parts (b),(c) clearly show that nonfractal filaments of the boundary come close to the fractal ones even on very fine scales. (d) The $x_{in} = -1.2$ boundary at time $t = 0.3$ obtained by marking the initial points "black" or "white," depending on whether the trajectories cross the $x = -1.2$ line in the upper or lower half-plane, respectively. Observe the absence of a pronounced band structure below and above the cylinder.

position "white" or "black," depending on whether in the time reversed dynamics on the stroboscopic map, after crossing the vertical line $x = x_{in}$, they lie above or below the $x$ axis, respectively. This implies choosing $y_c = 0$.

Figure 3(a) shows the $x_{in} = -6$ boundary. It contains both a smooth and a fractal component that can clearly be seen in the enlargements of Figs. 3(b) and 3(c), too. A remarkable feature is the pronounced band structure below and above the cylinder. To understand it let us recall that the boundary between the black and white regions is the image of the partitioning line $\{-\infty < x \leq -6, y = 0\}$. The boundary around the cylinder contains all the images of this line taken at any multiple of the period. The deviation of the boundary from the symmetry axis ($y = 0$) becomes non-negligible for $x > -2$ [cf. Fig. 3(a)]. This is because the model equations describe a nonstationary velocity field in front of the cylinder. The boundary strongly oscillates in front of the first stagnation point located around $x = -1$, $y = 0$. The bands observed above and below the cylinder are the images of this part

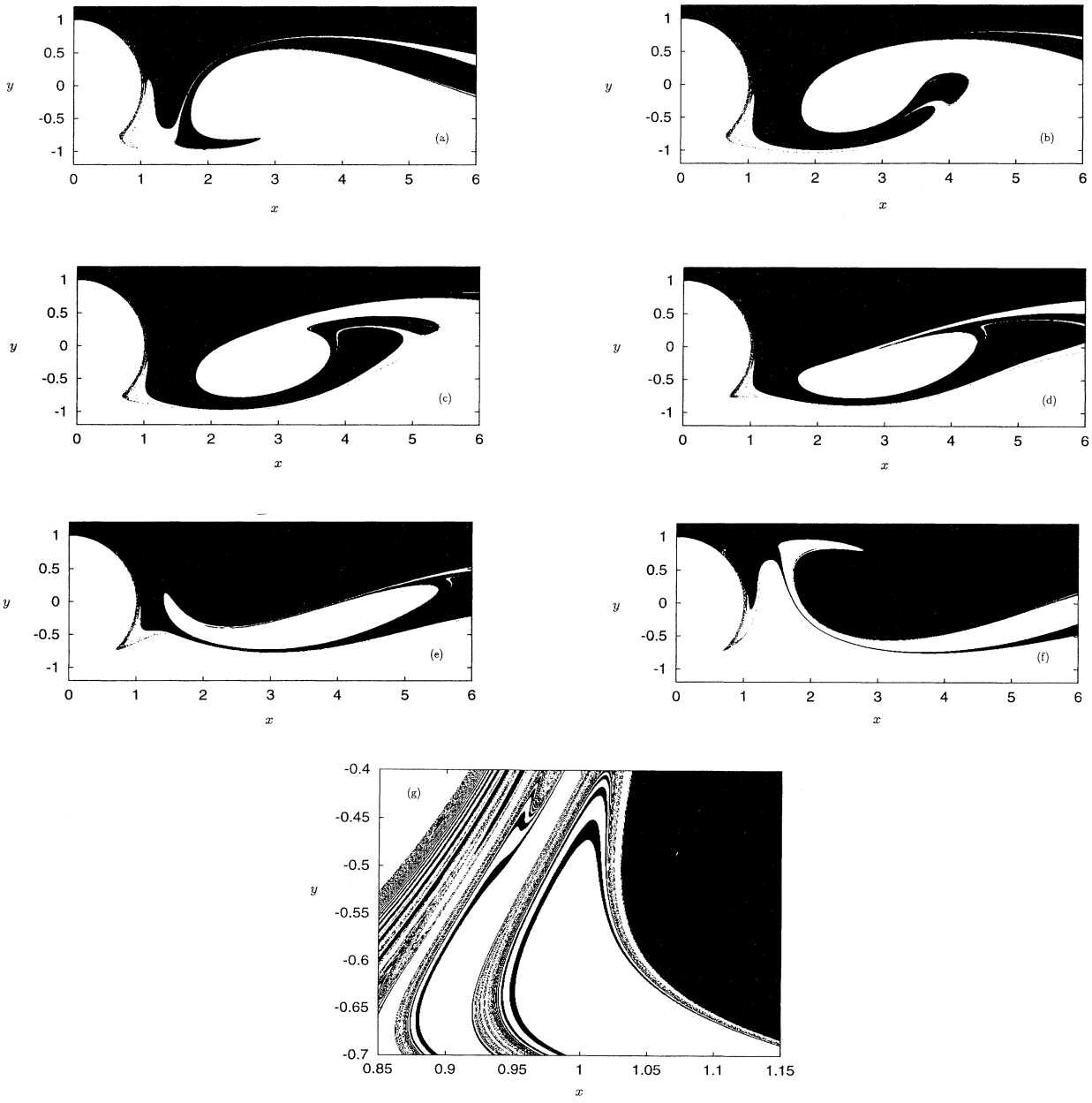


FIG. 4. The $x_{in} = 0$ boundary in experiment A [version (ii)] with $y_c = 0$. Particles were started on a grid of 800 × 400, but now they are colored depending on whether they pass "above" or "below" the cylinder. Parts (a)–(f) show the snapshots taken at equal times $t = n/10$, $n = 0, .., 5$ during half a period, $t \leq 0.5$. In the second half-period the corresponding figures can be obtained by performing the transformation $y \to -y$ and "black" $\leftrightarrow$ "white" [compare (a) and (f)]. (g) Enlargement of the boundary at $t = 0.3$ in the same range as in Fig. 3(b).

of the boundary [cf. Fig. 2(b)]. The fact that the band structure is more pronounced around the cylinder than around other parts of the boundary is a consequence of the anomalously slow convergence to the cylinder's surface that accumulates an infinity of parabolic points of the advection problem [8,9].

To study the dependence of the pattern on the choice of $x_{in}$, consider now the $x_{in} = -1.2$ boundary. In Fig. 3(d) one can observe that the strips have disappeared. This is because the streak line passing through $(-1.2, 0)$ only oscillates very close to the cylinder surface so that the images of this oscillating part cannot be seen in the resolution of the plot. The difference between Figs. 3(a) and 3(d) illustrates that the nonfractal part of the boundary depends on the choice of the initial line if the latter is taken in the nonasymptotic region.

In Figs. 4(a)–4(f) the $x_{in} = 0$ boundary is shown along with the time evolution of this boundary during half a period. We have chosen this boundary for plotting the time evolution because the fractal component appears most clearly in this case. Figure 4(g) displays an enlargement of the boundary in the same region as Fig. 3(d). Note the slight difference between the two patterns.

For comparison the unstable manifold of a period-1 orbit is shown in Fig. 5(a), which manifold also appears fully or partially in the Figs. 4 and 5. This supports the result that the $x_{in}$ boundary contains the unstable manifold of the chaotic set (which practically coincides with that of any periodic orbit).

Although this is a further extension of the same concepts, we find it worthwhile investigating $x_{in}$ boundaries with inflow lines taken *behind* the cylinder. Figure 6 displays the $x_{in} = 1.2$ boundary. In this range of $x_{in}$ versions (i) and (ii) are not equivalent, and we therefore show in parts (a) and (b) the boundary obtained by means of methods (i) and (ii), respectively. Although the fractal part of the two plots is the same, method (i) provides us with black points between the cylinder surface and the $x_{in} = 1.2$ line due to a back flow on this line. A closer investigation proves that the boundary contains a fractal part in the range $x \geq 3$ that seems to be very similar to that of Fig. 4(d). The fractal property with an initial line so far away downstream is at first glance surprising. Its presence can, however, be understood by looking at the detailed structure of the underlying chaotic saddle.

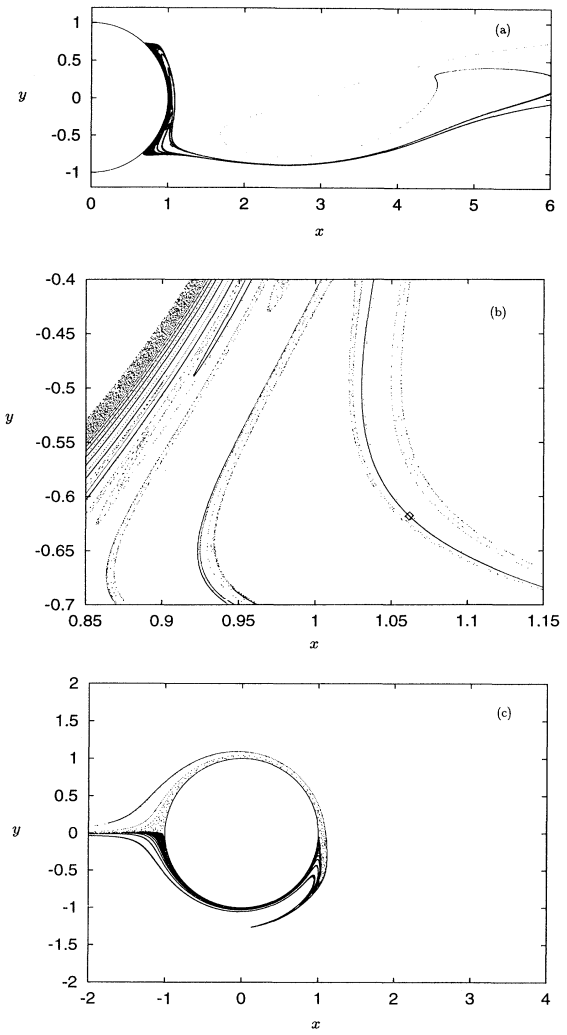


FIG. 5. Invariant manifolds of a period-1 orbit $x_0 = 1.064$, $y_0 = -0.621$ [small diamond in (b)] of eigenvalue $\simeq 24$ on the main set: The snapshot is taken at time $t = 0.3$. These manifolds provide a good approximation to those of the full chaotic saddle. (a) Unstable manifold in the region of Fig. 4. (b) Enlargement in the region of Fig. 3(b). The rightmost branch of the manifold does not appear as a part of the boundary shown in Fig. 3(b) because of the finiteness of the grid used there. (c) The stable manifold.

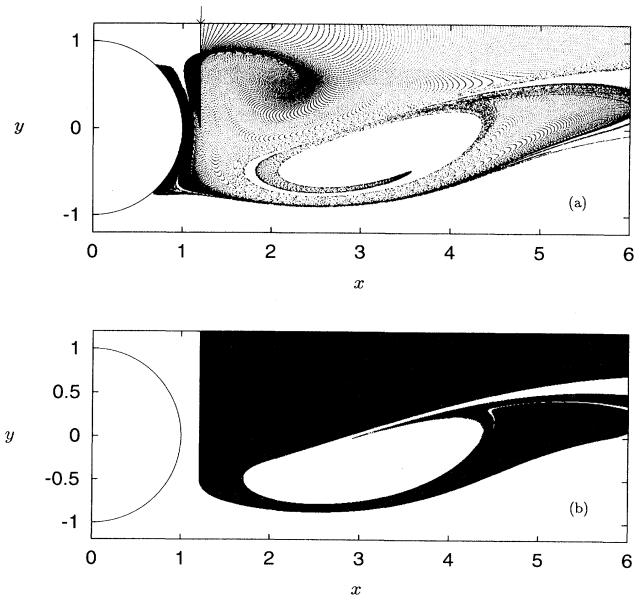


FIG. 6. The $x_{in} = 1.2$ boundary at $t = 0.3$ in experiment A. Part (a) [version (i)] has been plotted by injecting black tracers along the line segment $\{x = 1.2, 0 < y \leq 4\}$ marked by the arrow. Instead of a continuous injection, a discrete one was carried out with frequency 400/period. Part (b) [version (ii)] was obtained by the same method as Figs. 3(a) and 4.

### B. The chaotic saddle

We determine the chaotic saddle by means of the PIM triple method, and the result at time $t = 0.3$ is exhibited in Fig. 7(a). In order to avoid an overaccummulation of points on the cylinder surface, we use a slightly modified version of the original algorithm by choosing PIM triples at random, as worked out for generic Hamiltonian systems [22]. The plot shows that the set can be divided into different parts.

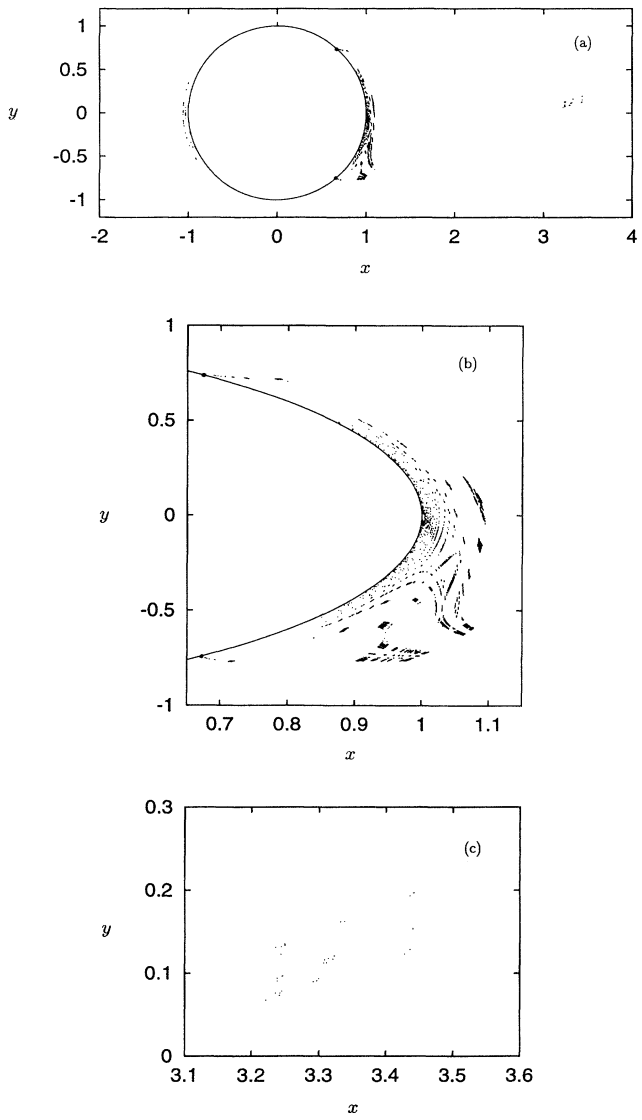


FIG. 7. The full chaotic saddle taken at $t = 0.3$ determined by means of the PIM triple algorithm. (a) The set can be divided into three parts: (i) A very thin part in front of the cylinder, the upstream set; and (ii) a bigger part that is close to the cylinder on the rear side, the main set. The two repelling stagnation points at $y = \pm 0.739$ (black dots) are corner points of this set, and their unstable manifolds form the outer boundary of the set. Note that the entire surface between the repelling stagnation point seems to belong to the main set. Because of the parabolic points on the surface, the main set has a strongly nonhyperbolic component. (iii) A far away part that is very rare, unstable, and seems to be hyperbolic with a complete ternary organization, the downstream set. (b) Enlargement of the main set. (c) Enlargement of the downstream set.

The dominant part, called the *main set*, is located just behind the cylinder in the range $x < 1.1$ [for an enlargement, see Fig. 7(b)]. It plays a basic role in the mixing and chaotic behavior in the wake of the cylinder. This part is bounded by the unstable manifold emanating from the repelling stagnation points on the upper and lower surfaces of the cylinder. These stagnation points [black dots in Fig. 7(a) at $x \simeq 0.67$] have been shown to be stationary in time [6]. Their positions can be determined numerically by distributing particles along a circle that is concentric with the cylinder whose radius is $1+\epsilon$. Constructing an azimuthal map telling us how the angular positions of such trajectories change after one period, two attracting fixed points appear. When letting $\epsilon$ approach zero, these fixed points become marginally stable and correspond to the stagnation points.

The main set contains both a *hyperbolic component*, based on strictly unstable periodic orbits lying off the immediate vicinity of the cylinder surface and a *nonhyperbolic component*, containing orbits coming arbitrarily close to the surface [8]. In fact the latter component seems to accumulate on the surface, between the two repelling stagnation points [9].

Another part of the chaotic set is located far away downstream around $x = 3$, and we call it the *downstream set*. As the enlargement of Fig. 7(c) shows, this part is rather rarefied and appears to be the direct product of two three-scale Cantor sets, slightly deformed on the $(x, y)$ plane. Dynamically, this part is fully hyperbolic, containing strongly unstable periodic orbits. The downstream set seems to have a stable manifold that is distinct from that of the main set, but in certain regions it is close to the latter one. This means that the two saddles have different incoming flows. The main set's stable manifold, however, does not penetrate into the region $x > 1.1$. In view of this observation, we can identify the fractal part of the $x_{in} = 1.2$ boundary as the unstable manifold of the downstream set. If the downstream set were not present, this boundary would be nonfractal. Figure 8 displays the invariant manifolds of a periodic orbit of the downstream set. It is easy to check that the unstable manifold of it is contained in Fig. 6.

Figure 7(a) also shows that there are PIM triple points in front of the cylinder, too, in the range $x > -1.1$. They form a tiny fractal set that will be called the *upstream set*. Its appearance is due to an untypical feature of the model: a backflow in a narrow range in front of the cylinder. Its size is much smaller than that of the main set but its dynamical and fractal properties are similar. The upstream and the main sets seem to have different incoming flows too, but both stable manifolds lie around the $x$ axis in front of the cylinder. In addition, the unstable manifold of the upstream set seems to accumulate on the cylinder surface, and comes arbitrarily close to the unstable manifold of the main set. Patterns connected with the unstable manifold of the upstream set cannot

be present on the $x_{in} = 0$ or $x_{in} = 1.2$ boundary but can on the $x_{in} = -1.2$ or $x_{in} = -6$ boundary. Because of the smallness of the upstream set, such a difference can only be seen in enlargements [cf. Figs. 3(b) and 4(g)]. We attribute the missing of the fractal part from Fig. 4(g) to the unstable manifold of the upstream set.

The stable manifolds of the upstream, main, and downstream sets go out to minus infinity along the $x$ axis. Therefore, a line $\{y_c = 0, x < x_{in}\}$ will be mapped close to the upstream set where some branches of the other two sets' stable manifold are also located. Consequently, the $x_{in} \ll 1$ boundaries contain all three of the unstable manifolds like, e.g., in Fig. 3.

Finally, it is worth mentioning that there could exist regions of bounded tracer motion of finite area embedded in the chaotic saddle. These are regions that cannot be reached by dye particles injected into the flow in front of the cylinder. While the downstream set seems to be fully hyperbolic with a complete symbolic encoding, the two other ones are certainly not. Therefore they could coexist with elliptic periodic orbits, but numerically we have not found any sign of these orbits with the resolution used.

### C. Experiment B

We start particles on a grid of $800 \times 666$ points [in the rectangle shown in Fig. 3(d)], follow their forward dynamics in the stroboscopic map, and mark them "black" or "white," depending on whether, after crossing the $x_{out} = 6$ line, they lie in the upper or lower half-plane, respectively ($y_c = 0$). The boundary shown in Fig. 9 has a fractal structure. We also plot the time evolution of the boundary within half a period. A comparison of Fig. 9(c) with Figs. 5(c) and 8(b) clearly shows that the stable manifolds of the main and downstream sets are contained in the boundary, but the same could be said about the upstream sets' stable manifold (not shown). This is so because the line $\{y_c = 0, x > x_{out} = 6\}$ intersects all three sets' unstable manifold. The shape of the boundary depends on $x_{out}$ if it is no longer far away from the cylinder. Had we taken the line of the outflow coordinate $x_{out}$ to be so close to the cylinder that could not be reached by the unstable manifold of the downstream set, the fractal component associated with this set's stable manifold would have disappeared. Similarly, on the $x_{out} = 0$ boundary the fractal component can only be associated with the stable manifold of the upstream set. Because of its smallness, this boundary (not shown) is invisible with the resolution used in the previous figures.

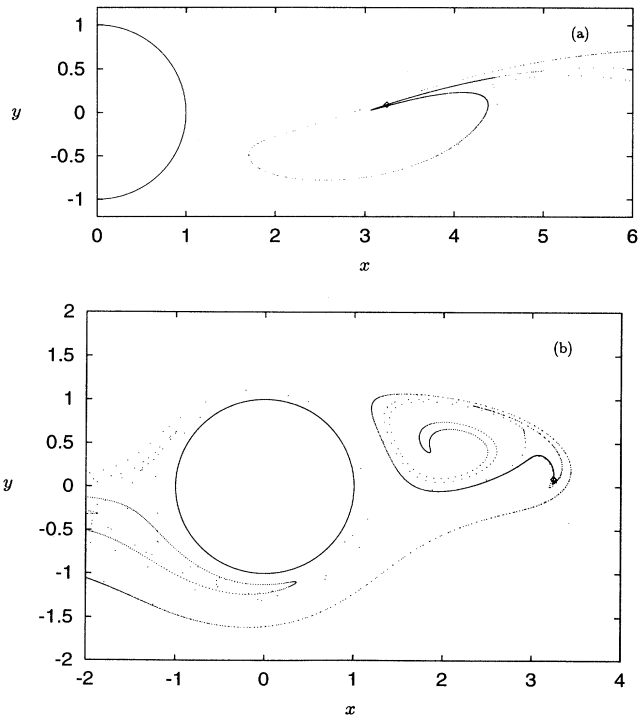


FIG. 8. The invariant manifolds of a period-1 orbit $x_0 = 3.245$, $y_0 = 0.093$ (small diamond) of eigenvalue $\simeq 105$ that closely approximate the unstable manifold of the downstream set. The snapshot is taken at time $t = 0.3$. (a) The unstable manifold in the full region of Fig. 4. (b) The stable manifold.

### D. Fractal properties

A quantitative measure of the fractality of the manifolds can be obtained by computing the so-called uncertainty exponent [15]. Take a segment crossing the $x_{in}$ or $x_{out}$ boundary transversally and divide it into small bins of size $\epsilon$. The uncertainty exponent shows how the fraction $f$ of uncertain boxes scales with $\epsilon$ (i.e., $f \sim \epsilon^{\alpha}$). We call a box uncertain if trajectories started from it go in the backward (direct) dynamics to both of the inflow (outflow) regions $y > y_c$ and $y < y_c$ at $x = x_{in}$ ($x_{out}$) (i.e. it contains both black and white points). The fractal dimension of the intersection is then $1-\alpha$. In our numerical computations we distributed randomly a large number of points $x_0$ in the interval considered. For each point $x_0$ we chose at random another one, $y_0$, in an interval of size $2\epsilon$ centered at $x_0$ to verify whether the box was uncertain. By taking the segment to be investigated as the right edge of the frame of Fig. 3(c), we have numerically found $\alpha = 0.39 \pm 0.02$. This yields for the fractal dimension of the $x_{in} = -6$ boundary $D_0 = 2 - \alpha = 1.61 \pm 0.02$. It is close to the value $D_0 = 1.65$ obtained for the fractal dimension of the stable manifold of the full saddle in Ref. [8], by means of a completely different method. By applying the same uncertainty analysis to a segment $\{x = 5,\ 0.47 < y < 0.49\}$ crossing the unstable manifold of the downstream set on the $x_{in} = 1.2$ boundary, we have obtained $\alpha = 0.74 \pm 0.02$. This implies that the fractal dimension of the unstable manifold of the downstream set is $D_0^{(d)} = 1.26 \pm 0.02$ and, consequently, that the downstream set has a smaller dimension than the main set. By comparing the uncertainty exponent of the $x_{in} = -6$ and $x_{in} = 0$ boundary we have not found any significant difference in the fractal dimension of the main and upstream sets. The fractal dimension of the full $x_{in}$ boundary for $| x_{in} | \gg 1$ is thus $D_0 = 1.61$ because the dimension of the union of several sets coincides with the

maximum of the components' dimensions.

Note that because of the Hamiltonian character of the Langrangian dynamics, the stable and unstable manifolds must have the same dimensions. The dimension of the full chaotic saddle is then $D_{saddle} = 2(D_0 - 1) = 1.22$ (while for the downstream set $D^{(d)}_{saddle} = 0.52$).

Thus we have shown that, if the inflow (outflow) line is taken in the asymptotic limit, the boundary in both experiments A and B have the same fractal dimension, that is, the same as the maximum dimension of the subsets' manifolds. In view of our statement that the fractal part of the boundary in experiment A (B) contains

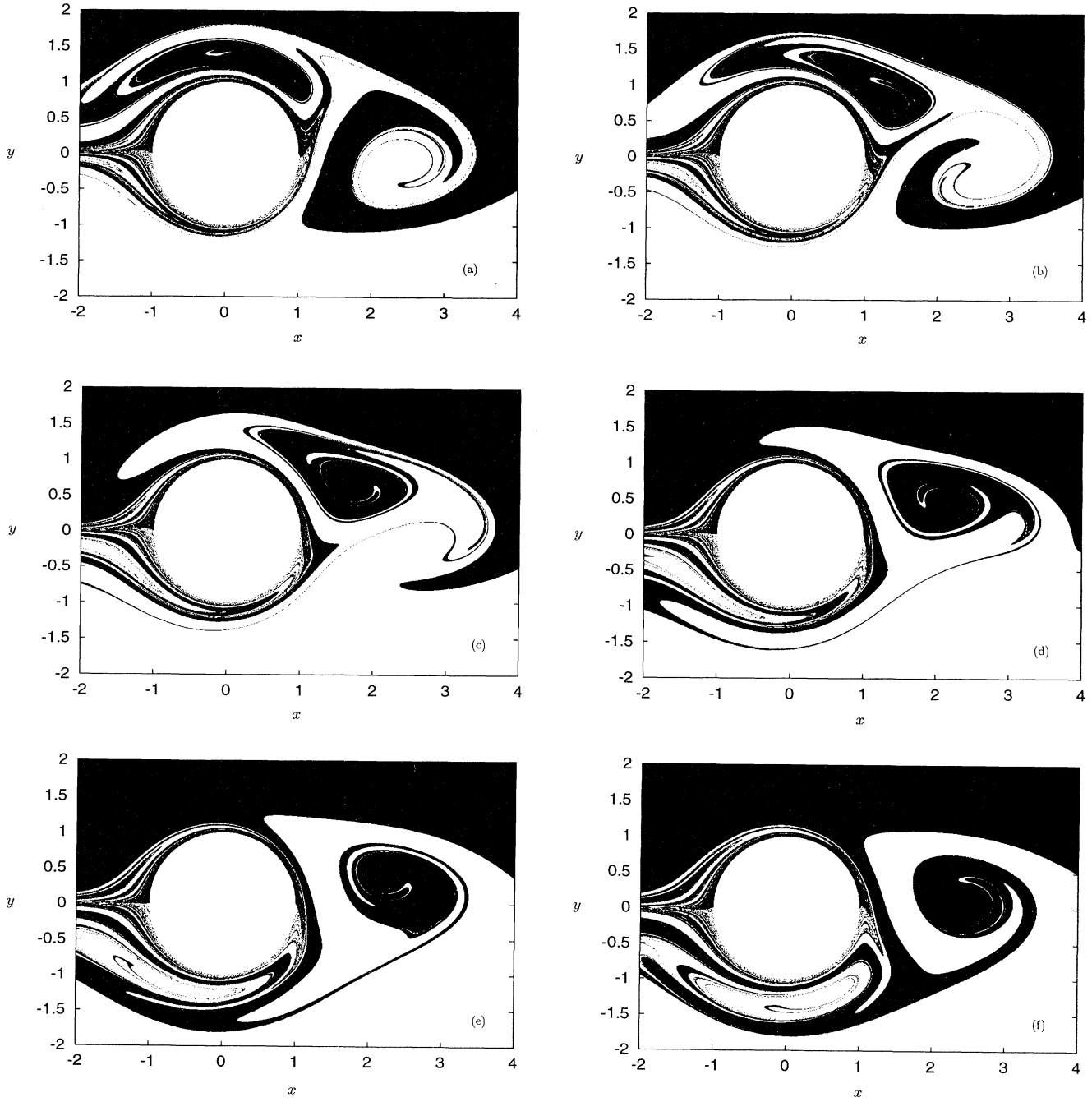


FIG. 9. The $x_{out} = 6$ boundary in experiment B with $y_c = 0$. Particles were started on an $800 \times 666$ grid in the rectangle shown and were marked "black" or "white" depending on whether, after crossing the $x = 6$ line in the stroboscopic map, they lie in the upper or lower half-plane, respectively. (a)–(f) The time dependence of the boundary is shown by taking snapshots at equal times $t = n/10$, $n = 0, \ldots, 5$ during half a period. In the second half-period the corresponding figures can be obtained by performing the transformation $y \to -y$ and "black" $\leftrightarrow$ "white" [compare (a) and (f)].

the unstable (stable) manifold, and these boundaries are streak lines, we can also say that the streak lines emanating from points far away from the cylinder in both experiments also have the same dimension $D_0$.

## V. CLOSING REMARKS

We have introduced the concept of $x_{in}$ and $x_{out}$ boundaries in the two-fluid and two-exit experiments, respectively, that can be carried out in open flows. If the tracer particles are passively advected (i.e., their inertia is negligible), we pointed out that these boundaries can be fractal boundaries exactly in the same sense as in dissipative dynamical systems. The condition for this is the existence of a chaotic saddle in the advection problem connected with the flow. The fractal component of the $x_{in}$ and $x_{out}$ boundaries contains then the unstable or the stable manifold of this set, respectively, or at least parts of them.

To illustrate the general concept and to reduce the amount of the numerics required, we considered an analytical model of a two-dimensional viscous flow around a cylinder. We emphasize that chaotic saddles persist under small changes in the flow (in the form of $\psi$) so we similarly expect Navier-Stokes flow to have chaotic saddles. For some values of the Reynolds number this has been numerically shown [10]. In our particular model the advection problem had various disjoint chaotic saddles. This phenomenon is of interest in itself and can typically occur in any Hamiltonian or dissipative system. As pointed out herewith, scanning a range of inflow or outflow conditions can lead in such cases to the analysis of certain parts of the full chaotic saddle. The difference among the fractal components of different $x_{in}$ or $x_{out}$ boundaries can only be understood in terms of the chaotic saddles' structures and their manifolds.

We indicated that the existence of an upstream set seems to be a peculiarity of the model. In other situations, however, like, e.g., when the obstacle is an oscillating cylinder or a rotating ellipsis, such a set can very well be present. As for the downstream set, the numerical investigations of the advection problem in a Navier-Stokes flow behind the cylinder [6–10] apparently do not indicate its presence. It could, however, be worth reconsidering these cases in the Navier-Stokes context with the aim of searching for such a set (which is expected to be rather unstable) with a better resolution.

It is finally worth emphasizing that the general scheme of boundaries introduced in this paper is not restricted to flows around obstacles. They can be defined for different cases when the flow is open with asymptotically simple velocity fields so that the particle dynamics can be considered as a scattering problem. An example can be the advection in the field of vortices forming a compact set while moving in a fluid, like, e.g., the leapfrogging of vortex rings or pairs [3,11]. More generally, fractal boundaries can be found in any open flow that is time periodic, even if the flow in the asymptotic region is not uniform. The analogy with scattering chaos is then lost but the existence of a chaotic saddle in Eq. (1) is still ensured, although the size of the regions in which fluid remains bounded for all time would be very likely non-negligible.

The visualization of open flows by means of streak lines has been a widespread method for decades [19]. The two-fluid experiment proposed in this paper provides an alternative method and sheds new light on this type of visualization. The two-exit experiment has no previously used counterpart at all, and is equivalent to constructing streak lines in the time reversed Lagrangian dynamics. Although the latter seems to be unrealistic in a laboratory, experiment B can be carried out with modern video techniques. The two experiments proposed provide us with information about two different sides of the dynamics: direct and backward, or stable and unstable features of the chaotic set.

The aim of this paper was to show that experimentalists can detect the existence of a chaotic saddle in the tracer dynamics by pointing out the fractal structure of the boundary between regions that are colored differently. Unfortunately, experiments A and B do not provide a direct way to detect the saddle itself. Taking the intersection of the $x_{in}$ and $x_{out}$ boundaries, it certainly contains points of the saddle but many others, too, because of the nonfractal part of the boundary. We briefly mention that with some modification, experiments A and B could lead to a determination of the manifolds. By interrupting the injection of the colored fluid in experiment A, the nonfractal part of the boundary (that is not on an invariant curve) is transported away by the flow and after some time dye particles of any color will trace out the unstable manifold. This is equivalent to studying the pattern to which streak lines of finite length converge as proposed in [9,10]. Analogously, if in experiment B we save only those points (again of any color) that do not leave a region around the obstacle earlier than a given number $n$ times the period, the stable manifold will be traced out for increasing $n$. Since to our knowledge not even streak line patterns have been analyzed from the point of view of dynamical system theory in a laboratory experiment, the realization of the experiments proposed in the paper could lead to a better understanding of classical hydrodynamical problems.

## ACKNOWLEDGMENTS

This work has been partially supported by the Hungarian Science Foundation Grants Nos. OTKA 2090, T4439, F4286, by the Foundation for Hungarian Higher Education and Research, by the PHARE ACCORD program H9112-0378, by the U.S.-Hungarian Science and Technology Joint Founds under Project 286, by the National Science Foundation (Division of Mathematical and Physical Science), and by the Department of Energy (Office of Scientific Computing). Z.T. is grateful for the kind hospitality at Institute for Plasma Research, University of Maryland, College Park.

[1] J. M. Ottino, *The Kinematics of Mixing: Stretching, Chaos and Transport* (Cambridge University Press, Cambridge, 1989); A. Crisanti, M. Falcioni, G. Paladin, and A. Vulpiani, Riv. Nuovo Cimento **14**, 207 (1991); F. J. Muzzio, P. D. Swanson, and J. M. Ottino, Int. J. Bifurc. Chaos **2**, 37 (1992).
[2] S. Jones and H. Aref, Phys. Fluids **31**, 469 (1988).
[3] K. Shariff, A. Leonard, N. J. Zabusky, and J. H. Ferziger, Fluid Dyn. Res. **3**, 337 (1988).
[4] K. Shariff and A. Leonard, Annu. Rev. Fluid Mech. **24**, 235 (1992).
[5] V. Rom-Kedar, A. Leonard, and S. Wiggins, J. Fluid Mech. **214**, 347 (1990).
[6] K. Shariff, T. H. Pulliam, and J. M. Ottino, Lect. Appl. Math. **28**, 613 (1991).
[7] C. Jung and E. Ziemniak, J. Phys. A **25**, 3929 (1992).
[8] C. Jung, T. Tél, and E. Ziemniak, Chaos **3** 555 (1993).
[9] E. Ziemniak, C. Jung, and T. Tél, Physica D **76**, 123 (1994).
[10] C. Jung and E. Ziemniak, in *Fractals in the Natural and Applied Physical Sciences*, edited by M. M. Novak (North-Holland, Amsterdam, 1994).
[11] Á. Péntek, T. Tél, and Z. Toroczkai (unpublished).
[12] U. Smilansky, in *Chaos and Quantum Physics*, edited by M. J. Giannoni *et al.* (Elsevier Science, New York, 1992).
[13] C. Jung, Acta Phys. Polon. **23**, 177 (1992); E. Ott and T. Tél, Chaos **3**, 417 (1993).
[14] C. Grebogi, E. Ott, and J. A. Yorke, Physica D **7**, 181 (1983); H. Kantz and P. Grassberger, *ibid.* **17**, 75 (1985); G. H. Hsu, E. Ott, and C. Grebogi, Phys. Lett. **127A**, 199 (1988); T. Tél, in *Directions in Chaos*, edited by Hao Bai-lin (World Scientific, Singapore, 1990), Vol. 3, pp. 149–211.
[15] C. Grebogi, S. W. McDonald, E. Ott, and J. A. Yorke, Phys. Lett. **99A**, 415 (1983); S. W. McDonald, E. Ott, and J. A. Yorke, Physica D **17**, 125 (1985).
[16] C. Grebogi, E. Ott, and J. A. Yorke, Phys. Rev. Lett. **50**, 935 (1983); **56**, 1011 (1986); C. Grebogi, E. Kostelich, E. Ott, and J. A. Yorke, Physica D **25**, 347 (1987).
[17] H. Aref, S. W. Jones, S. Mofina, and I. Zawadski, Physica D **37**, 423 (1989).
[18] S. Bleher, C. Grebogi, E. Ott, and R. Brown, Phys. Rev. A **38**, 930 (1988).
[19] M. Van Dyke, *An Album of Fluid Motion* (The Parabolic Press, Stanford, 1982).
[20] I. M. Jánosi, L. Flepp, and T. Tél, Phys. Rev. Lett. **73**, 529 (1994).
[21] H. E. Nusse and J. A. Yorke, Physica D **36**, 137 (1989).
[22] Z. Kovács and L. Wiesenfeld (unpublished).

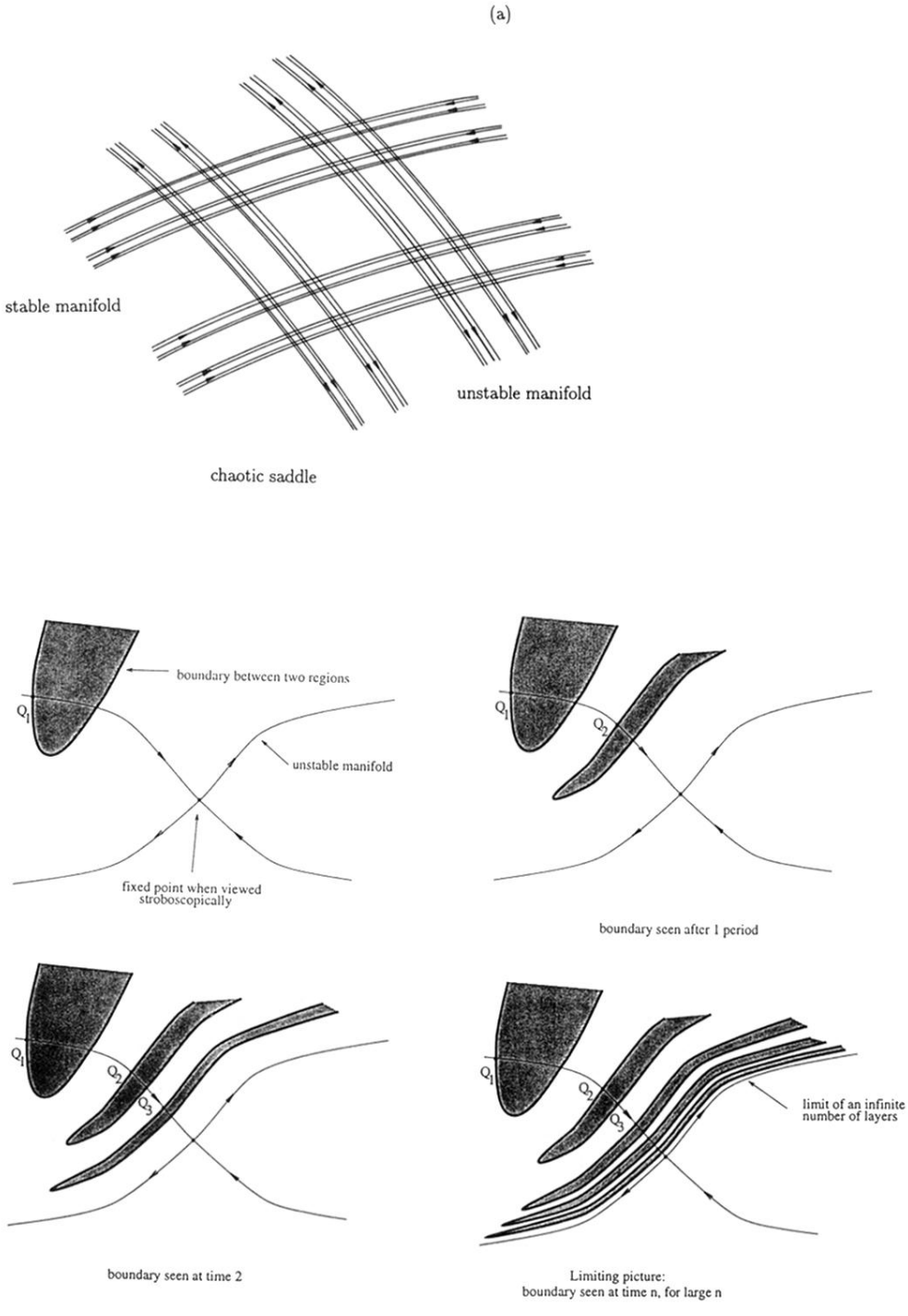


FIG. 2. Schematic diagram illustrating the convergence to the chaotic saddle of a general Hamiltonian system. (a) The chaotic saddle and its stable and unstable manifolds. A finite segment of the partitioning line (not shown) would be smoothly deformed before reaching the chaotic set. Points lying on the stable (unstable) manifold remain, however, glued to the set forever. Segments in between become more and more elongated, transported out to infinity so that they converge to the unstable (stable) manifold. (b) The evolution of the local structure of the boundary between two incoming regions black (B) and white (W) on a stroboscopic map when the partitioning line crosses the stable manifold of a fixed point. Once $Q_1$ is on the boundary, so must $Q_2, Q_3, \ldots$ be also on the boundary; thus the fixed point's unstable manifold is the limit of an infinite number of layers of the boundary. An analogous structure is built up in the $x_{in}$ boundary of the hydrodynamical experiment A around the chaotic saddle's unstable manifold.